Accepted Manuscript

Galectin-3 is essential for proper bone cell differentiation and activity, bone remodeling and biomechanical competence in mice

Carla Iacobini, Claudia Blasetti Fantauzzi, Rossella Bedini, Raffaella Pecci, Armando Bartolazzi, Bruno Amadio, Carlo Pesce, Giuseppe Pugliese, Stefano Menini

PII: S0026-0495(18)30040-4
DOI: https://doi.org/10.1016/j.metabol.2018.02.001
Reference: YMETA 53737

To appear in:

Received date: 30 October 2017
Accepted date: 3 February 2018

Please cite this article as: Carla Iacobini, Claudia Blasetti Fantauzzi, Rossella Bedini, Raffaella Pecci, Armando Bartolazzi, Bruno Amadio, Carlo Pesce, Giuseppe Pugliese, Stefano Menini , Galectin-3 is essential for proper bone cell differentiation and activity, bone remodeling and biomechanical competence in mice. The address for the corresponding author was captured as affiliation for all authors. Please check if appropriate. Ymeta(2018), https://doi.org/10.1016/j.metabol.2018.02.001

Galectin-3 is essential for proper bone cell differentiation and activity, bone remodeling and biomechanical competence in mice

Running title: Essential role for Galectin-3 in bone remodeling and competence

Carla Iacobini [1], Claudia Blasetti Fantauzzi [1], Rossella Bedini [2], Raffaella Pecci [2], Armando Bartolazzi [3,4], Bruno Amadio [5], Carlo Pesce [6], Giuseppe Pugliese [1*], and Stefano Menini [1]

[1] Department of Clinical and Molecular Medicine, "La Sapienza" University, 00189 Rome, Italy; [2] National Centre of Innovative Technologies in Public Health, Italian National Institute of Health, 00161 Rome, Italy; [3] Laboratory of Surgical and Experimental Pathology, Sant'Andrea University Hospital, 00189 Rome, Italy; [4] Department of Oncology-Pathology, Cancer Center Karolinska Universitetssjukhuset Solna, S-17176 Stockholm, Sweden; [5] SAFU Laboratory, Department of Research, Advanced Diagnostics, and Technological Innovation, Translational Research Area, Regina Elena National Cancer Institute, 00144 Rome, Italy; and [6] DINOGMI, University of Genoa Medical School, 16132 Genoa, Italy.

*** Corresponding author:**

Giuseppe PUGLIESE, MD, PhD

Department of Clinical and Molecular Medicine

Via di Grottarossa, 1035-1039 - 00189 Rome, Italy

Phone: +39-0633775440; Fax: +39-0633776327

E-mail: giuseppe.pugliese@uniroma1.it

Word counts: abstract 330 words; text 4,869 words (including the abbreviation list, acknowledgements, funding, disclosure statement, and author contributions).

Abstract

Objective. Galectin-3 is constitutively expressed in bone cells and was recently shown to modulate osteogenic transdifferentiation of vascular smooth muscle cells and atherosclerotic calcification. However, the role of galectin-3 in bone physiology is largely undefined. To address this issue, we analyzed (1) the skeletal features of 1-, 3- and 6-month-old galectin-3 null (*Lgals3*$^{-/-}$) and wild type (WT) mice and (2) the differentiation and function of osteoblasts and osteoclasts derived from these animals.

Methods. Long bone phenotype, gene expression profile, and remodeling were investigated by micro-computed tomography, real time-PCR, static and dynamic histomorphometry, and assessment of biochemical markers of bone resorption and formation. Bone competence was also evaluated by biomechanical testing at 3 months. *In vitro*, the effects of galectin-3 deficiency on bone cell differentiation and function were investigated by assessing (a) gene expression of osteoblast markers, alkaline phosphatase activity, mineralization assay, and WNT/β-catenin signaling (of which galectin-3 is a known regulator) in osteoblasts; and (b) tartrate-resistant acid phosphatase activity and bone resorption activity in osteoclasts.

Results. *Lgals3*$^{-/-}$ mice revealed a wide range of age-dependent alterations including lower bone formation and higher bone resorption, accelerated age-dependent trabecular bone loss ($p< 0.01$ vs. WT at 3 months) and reduced bone strength ($p<0.01$ vs. WT at 3 months). These abnormalities were accompanied by a steady inflammatory state, as revealed by higher bone expression of the pro-inflammatory cytokines interleukin (IL)-1β and IL-6 ($p<0.001$ vs. WT at 3 months), increased content of osteal macrophages ($p<0.01$ vs. WT at 3 months), and reduced expression of markers of alternative (M2) macrophage activation. *Lgals3*$^{-/-}$ osteoblasts and osteoclasts showed impaired terminal differentiation, reduced mineralization capacity ($p<0.01$ vs. WT cells) and resorption activity ($p<0.01$ vs. WT cells). Mechanistically, impaired

differentiation and function of *Lgals3*$^{-/-}$ osteoblasts was associated with altered WNT/β-catenin signaling ($p<0.01$ vs. WT cells).

Conclusions. These data provide evidence for a contribution of galectin-3 to bone cell maturation and function, bone remodeling, and biomechanical competence, thus identifying galectin-3 as a promising therapeutic target for age-related disorders of bone remodeling.

Key words: galectin-3; bone remodeling; bone strength; osteoblasts; osteoclasts; macrophages.

Nonstandard abbreviations used: VSMCs = vascular smooth muscle cells; *Lgal-3*$^{-/-}$ = galectin-3 knockout; Runx2 = Runt-related transcription factor 2; WT = wild type; μCT = micro-computed tomography; BV/TV = bone volume/total tissue volume; Tb.Th = trabecular thickness; Tb.N = trabecular number; Tb.Sp = trabecular separation; Ct.Th = cortical thickness; TA = total area; BA = cortical bone area; TA/BA = bone area fraction ; Ix = area moment of inertia; N.Oc/B.pm = osteoclast number/bone perimeter; IHC = immunohistochemistry; TRAcP = tartrate-resistant acid phosphatase; N.Ob/B.pm =osteoblast number/bone perimeter; MAR = mineral apposition rate; ADGRE1 = Adhesion G Protein-Coupled Receptor E1; qRT-PCR; real time-PCR; ALPL = alkaline phosphatase; OCN = osteocalcin; RANKL = receptor activator of nuclear factor kappa-B ligand; OPG = osteoprotogerin; SOST = sclerostin; IL = interleukin; TGF = transforming growth factor; CTX = carboxy-terminal collagen crosslinks; ucOCN = undercarboxylated OCN; COL1A1 = collagen I; TCF/LEF = T-cell factor/lymphoid enhancer factor; M-CSF = macrophage colony-stimulating factor; N = number.

1. Introduction

Osteoporosis is a common disorder characterized by altered bone remodeling [1], the lifelong process by which bone is renewed to maintain bone mass. Bone remodeling involves finely orchestrated cellular and molecular events and is commonly viewed as a two-step process carried on by bone cells, with old bone resorption by osteoclasts followed by new bone formation by osteoblasts. These two events occur in a balanced and coordinated manner in order to maintain bone mass and shape largely unchanged throughout adult life [2,3]. Despite growing efforts, a vast gap remains in our understanding of bone remodeling, especially of the molecular regulators of differentiation and activity of osteoclasts and osteoblasts [4,5]. As knowledge advances, new therapeutic strategies may emerge to reduce the health burden and economic costs related to osteoporotic fractures, which are expected to increase in the future [5].

Galectin-3 is a 29- to 35-kDa protein constitutively expressed in various tissues [6] and involved in several physiological and pathological processes [7]. In particular, previous studies have shown that galectin-3 plays a role in diabetic complications [8], atherosclerosis [9,10], and other inflammatory conditions, including bone inflammatory disorders [11]. The link between galectin-3 and these pathological conditions lies in the role of this lectin in the modulation of the immune/inflammatory response [12], as evidenced by the numerous reports showing a regulatory activity on both innate and adaptive immune cells [13]. In particular, galectin-3 was shown to stimulate T-cell apoptosis [14], inhibit T-cell growth and T helper 1 differentiation [15,16], down-regulate T cell receptor-mediated T-cell activation [16], and induce alternative (M2) macrophage activation [17,18]. In quiescent cells, galectin-3 shows prominent cytoplasmic localization, whereas it is found predominantly in the nucleus of replicating cells [19]. Galectin-3 is also secreted into the extracellular space through a non-classical secretory pathway [20]. Here, it interacts with the β-galactoside residues of several glycoproteins, thus

forming higher order supramolecular structures resulting in galectin-ligand lattices on the cell surface [21]. The galectin-glycoprotein lattice has been shown to play a role in the regulation of receptor clustering, endocytosis and signaling, thereby controlling important cell functions such as cell transdifferentiation, migration and fibrogenesis [21-23].

Recently, we demonstrated a key role of galectin-3 in the processes of atherosclerotic vascular calcification and osteogenic transdifferentiation of vascular smooth muscle cells (VSMCs) to calcifying vascular cells. We showed that galectin-3 protein was highly expressed by VSMCs at the boundary of extensively calcified areas of human carotid plaques and that VSMCs isolated from galectin-3 knockout (*Lgal-3*$^{-/-}$) mice were unable to acquire a complete osteoblast-like phenotype and to produce organized calcifying nodules when cultured in an osteogenic medium [24]. These data indirectly reveal osteogenic properties of galectin-3, as also suggested by previous observations. Indeed, in the skeleton, the expression of galectin-3 was found to be under control of Runt-related transcription factor 2 (Runx2), the main regulator of osteoblast differentiation and activity during bone formation [25], and extracellular galectin-3 was shown to regulate osteoblast-osteoclast interaction [26]. Moreover, Colnot *et al.* demonstrated that galectin-3 is a marker of both chondrogenic and osteogenic cell lineages, thus suggesting that it might be involved in the process of endochondral bone formation. In addition, these Authors showed that galectin-3 is also expressed in osteoblasts and osteocytes of the woven trabecular and cortical bone, in osteoclasts at the front of ossification, and in mononuclear cells within bone marrow cavity [6,27]. Finally, the decrease of galectin-3 in the plasma of elderly individuals was shown to be associated with the age-related loss of osteogenic differentiation capacity of mesenchymal stem cells [28]. Despite this evidence, the specific role of galectin-3 in the age-dependent regulation of bone mass and the modulation of bone cells differentiation/maturation and activity has not been thoroughly investigated.

These *in vivo* and *in vitro* studies were aimed at addressing this issue by analyzing the bone phenotype of *Lgal-3*$^{-/-}$ mice as well as the differentiation and function of osteoblasts and osteoclasts derived from these animals.

2. Materials and methods

2.1. *In vivo* analysis of skeletal phenotype and bone turnover

2.1.1. Design. The study protocol was approved by the Institutional Animal Care of the Regina Elena National Cancer Institute and by the National Ethics Committee for Animal Experimentation of the Italian Minister of Health (D.lgs. 26/2014, Act n°184). The animals were housed and cared according to standards articulated in the "Animal Research: Reporting of In Vivo Experiments" (ARRIVE) (https://www.nc3rs.org.uk/arrive-guidelines) guidelines and to the national laws and regulations and received water and food *ad libitum*. Female C57/BL6 wild type (WT) and *Lgals3*$^{-/-}$ mice on the same background were sacrificed at 1, 3 and 6 months of age. Seven 1- and 3-month old and six 6-month old animals per each genotype were used.

2.1.2. Micro-computed tomography. Micro-computed tomography (μCT) was performed in right femurs using a Skyscan 1072 microtomography system (Bruker microCT, Kontich, Belgium). The cross-section reconstruction was performed using the CONE BEAM Reconstruction version 2.23 software (Bruker microCT) [29]. Bones from WT and *Lgals3*$^{-/-}$ mice aged 1, 3 and 6 months were examined. Trabecular bone architecture was evaluated at the distal femoral metaphysis following the procedures described by Boxsein *et al*. [30] for scan acquisition and computing of the following morphometric parameters: bone volume/total tissue volume (BV/TV, %), trabecular thickness (Tb.Th, μm), trabecular number (Tb.N, mm^{-1}), and trabecular separation (Tb.Sp, μm). Moreover, at the femoral midshaft, 50 transverse CT slices were obtained and used to compute cortical thickness (Ct.Th, μm), total area (TA, mm^2),

cortical bone area (BA, mm^2), and bone area fraction (TA/BA, %). Finally, the area moment of inertia (Ix, mm^4) was calculated from the geometrical parameters obtained by μCT.

2.1.3. Femur biomechanical testing. Bone bending strength was assessed by three-point bending test following the procedures described by Ritchie *et al.* [31]. Briefly, femurs of adult (aged 3 months) mice were tested in three-point bending on an M30K testing machine (Lloyd Instruments Ltd., Bognor Regis, UK), equipped with a 50 N load cell and a custom bone supports with 8 mm distance gauge length. Femurs were loaded with the posterior surface in tension. Load was applied at a constant rate of 1 mm/min until failure. The failure load (i.e., the ultimate force needed to break the femur) was recorded by the testing machine and the NEXYGEN v4.5 Materials Testing Software (Lloyd Instruments Ltd.), according to D790 of the American Society for Testing and Materials [32] and expressed in N.

2.1.4. Bone histomorphometry and immunohistochemistry. Left femurs and tibiae from WT and *Lgals3*$^{-/-}$ mice were fixed in 4% paraformaldehyde. Femurs were dehydrated in acetone and processed for glycol–methacrylate embedding (Technovit 8100, Bio-Optica, Milan, Italy) without decalcification, whereas tibiae were paraffin embedded after 10-14 days decalcification with 10% EDTA pH 7.2-7.4. Tissue morphology was assessed by hematoxylin-eosin staining. Static and dynamic histomorphometric measurements were carried out on 5 μm–thick sections with the interactive image analyzer Image-Pro Premier 9.2 (Immagini&Computer, Milan, Italy) and using the suggested nomenclature [33]. Osteoclast number/bone perimeter (N.Oc/B.pm) was evaluated after immunohistochemistry (IHC) staining of the sections for the activity of the osteoclast marker tartrate-resistant acid phosphatase (TRAcP) (kit #387A-1KT, Sigma-Aldrich, St.Louis, MO, USA). Osteoblast number/bone perimeter (N.Ob/B.pm) was evaluated after staining the sections with methylene blue/azure II (Sigma-Aldrich). Dynamic assessment of trabecular bone formation was performed by injecting mice with calcein (10 μg/g body weight i.p.; Sigma-Aldrich) 10 and 3 days before

sacrifice [2] and then evaluating double calcein labeling under the fluorescence microscope (Olympus BX51, Olympus Italia S.R.L., Segrate, Italy). Mineral apposition rate (MAR) was then calculated as the distance between the midpoints of two consecutive labels, divided by the time period between the two injections and expressed as μm/day [33]. The content of osteal tissue macrophages was also analyzed by IHC, using a rat monoclonal antibody to mouse cell surface glycoprotein F4/80 or Adhesion G Protein-Coupled Receptor E1 (ADGRE1) (NB 600-404, Novus Biologicals, Littleton, CO, USA) [34], a widely used murine monocyte/macrophage marker. Light micrographs of histological sections were acquired using a CCD camera module (JVC TK-C1380 Color Video Camera, Immagini&Computer) coupled to a Leights Eclipse ME600 microscope (Nikon Instruments Italia S.p.A, Firenze, Italy).

2.1.5. Analysis of bone tissue mRNA expression. Total RNA was extracted from the humeri and right tibias, after flushing of the bone marrow. The diaphysis was homogenized by means of a tissue homogenizer (Bullet Blender, Next Advance Inc., Troy, NY, USA), followed by total RNA isolation using Trizol Reagent (Thermo Fisher Scientific, Whaltam, MA, USA), according to the manufacturer's instructions. Expression of the following genes was assessed by quantitative real time-PCR (qRT-PCR) using a StepOne™ RT-PCR instrument (Applied Biosystems, Monza, Italy), as previously reported [34]: the osteoblast differentiation markers *Runx2*, alkaline phosphatase (*Alpl*), and osteocalcin (*Ocn*); the osteoclast differentiation marker *Trap*; the bone remodeling regulators receptor activator of nuclear factor kappa-B ligand (*Rankl*), osteoprotogerin (*Opg*), and sclerostin (*Sost*); the pro-inflammatory cytokines interleukin-6 (*Il6*) and interleukin-1β (*Il1b*); the macrophage marker F4/80 (*Adgre1*), the M2 macrophage marker transforming growth factor-β (*Tgfb*), and the M2 secreted cytokine interleukin-10 (*Il10*). Targets were quantified by TaqMan Gene Expression Assays (Applied Biosystems) using the assays reported in Supplementary Table 1.

2.1.6. Biochemical determinations. Serum was obtained from a blood sample collected at euthanasia after one night fasting. Serum TRAcP 5b, an osteoclast/bone resorption biomarker; carboxy-terminal collagen crosslinks (CTX), a marker of the degradation of mature type I collagen characterizing bone resorption; the bone formation marker OCN; and undercarboxylated OCN (ucOCN), resulting from the decarboxylation of the first glutamic acid residue of OCN incited by the low pH generated during bone resorption [35], were measured by ELISA using the following kits: mouse TRACP-5b kit (MyBioSource Inc., San Diego, CA, USA); mouse CTX-1 (Abbexa Ltd., Cambridge, UK); mouse Glu-Osteocalcin and Gla-Osteocalcin High Sensitive EIA Kits (Takara Bio Inc., Shiga, Japan), respectively.

2.2. *In vitro* analysis of osteoblastogenesis and osteoclastogenesis

2.2.1. Design. Osteoblast and osteoclast differentiation and function were assessed in calvarial osteoblast cultures and primary osteoclast cultures, respectively, isolated from WT and *Lgals3*$^{-/-}$ animals.

2.2.2. Calvarial osteoblast cultures. Calvariae removed from 7-day old WT and *Lgals3*$^{-/-}$ mice were cleaned free of soft tissues and digested three times with 1 mg/ml Clostridium histolyticum type IV collagenase (#17104019, Thermo Fisher Scientific) and 0.25% trypsin (#85450C, Sigma-Aldrich). Cells from the second and third digestions were plated and grown in DMEM plus 10% FBS. At confluence, cells were trypsinized and plated in standard medium (αMEM plus 10% FBS, Thermo Fisher Scientific) or osteogenic medium, i.e., standard medium supplemented with 10 mM β-glycerophosphate **(#**G6626, Sigma-Aldrich) and 50 μg/ml ascorbic acid (#A1300000, Sigma-Aldrich) for 4 weeks.

2.2.3. Gene expression of osteoblast markers. The mRNA expression levels of the genes coding for the osteoblast markers *Runx2*, *Alpl*, and *Ocn* were evaluated by qRT-PCR, along with those of *Rankl*, *Opg* and collagen I (*Col1a1*). Targets were quantified by TaqMan Gene Expression Assays (Applied Biosystems) using the assays reported in Supplementary Table 1.

2.2.4. ALP activity assay. The activity of ALPL was evaluated histochemically in WT and *Lgals3*$^{-/-}$ osteoblasts after 4 weeks of incubation in osteogenic medium, using the Alkaline Phosphatase Detection Kit (kit #85, Sigma-Aldrich) according to the manufacturer's instruction.

2.2.5. Mineralization assay. After 4 weeks of incubation in osteogenic medium, osteoblast monolayers were stained with the von Kossa method (#04170801, Bio-Optica) for calcium and Alizarin red (#A5533-25G, Sigma-Aldrich) to visualize mineralized nodules. Total mineralization area (%) and number and size of calcification nodules were assessed in monolayers stained with von Kossa using the Image-Pro Premier 9.2 image analyzer, as previously described [24]. Moreover, to account for calcium deposits not detectable at light microscopy analysis, total calcium content of monolayers was quantified using a colorimetric assay (Quantichrom Calcium Assay Kit, BioAssay Systems, Hayward, CA, USA), according to the manufacturer's instructions. Calcium content was normalized to total protein content, as assessed by Quick Start™ Bradford Protein Assay (Bio-Rad Laboratories S.r.l., Segrate, Italy).

2.2.6. WNT/β-catenin signaling pathway. Signaling through the WNT/β-catenin pathway was analyzed in osteoblast monolayers grown in osteogenic medium using the Cignal TCF/LEF Reporter Assay Kit #CCS-018 (Qiagen GmbH, Hilden, Germany), which contains a mixture of an inducible T-cell factor/lymphoid enhancer factor (TCF/LEF) transcription factor-responsive firefly luciferase reporter and a constitutively expressing Renilla luciferase construct, as per manufacturer's instructions. The luminescence reaction was monitored 48 hours post-transfection using the Dual Glo Luciferase Assay System #E2920 (Promega Co., Madison, WI, USA) and a Varioskan Lux Multimode Microplate Reader (Thermo Fisher Scientific). Luciferase activity was reported as relative light units of the firefly and renilla luciferase luminescence ratio after normalizing for transfection efficiency.

2.2.7. Primary osteoclast cultures. Bone marrow cells from hindlimbs of 6-week old WT and *Lgals3*$^{-/-}$ mice were diluted 1:1 in Hank's balanced salt solution and layered over Histopaque 1077 solution. Monocytes were isolated by gradient centrifugation. Cells were washed twice with Hank's solution, resuspended in DMEM plus 10% FBS and plated in culture dishes at a density of 10^6 cells/cm^2. After 3 days, cells were rinsed to remove non-adherent cells and cultured in osteoclastogenic medium, i.e. the same medium plus 50 ng/ml recombinant mouse macrophage colony-stimulating factor (M-CSF) (#M9170, Sigma-Aldrich) and 120 ng/ml recombinant mouse RANKL (#R0525, Sigma-Aldrich) for 7 days.

2.2.8 TRAcP activity. TRAcP activity was detected histochemically, using the Acid Phosphatase, Leukocyte (TRAP) Kit (kit #387A-1KT, Sigma-Aldrich). The number (N) of small (4 < nuclei), medium (4-10 nuclei), large (> 10 nuclei), and total TRAP-stained osteoclasts from long bones were assessed by counting cells in 5 random fields covering ~20 % of the total well surface, and expressed as N/well [36].

2.2.9 Bone resorption activity. Bone resorption activity was evaluated by culturing osteoclasts on bone slices (Osteo Assay Surface multiwell plates #CLS3987-4EA, Corning®, Sigma-Aldrich) under the same culture conditions described in 2.2.7., and evaluating the number of pits (areas of osteolysis) and total resorbed area after staining with 0.1% toluidine blue (#89640, Sigma-Aldrich), according to Caselli *et al* [37].

2.3. Statistical analysis

Results are expressed as mean±SD.

Statistical significance was evaluated by Student's t test or the corresponding Mann-Whitney U test, in case of variables with a skewed distribution.

A *P*-value <0.05 was considered significant. All statistical tests were performed on raw data.

3. Results

3.1. *Lgals3*$^{-/-}$ mice show altered skeletal phenotype, bone turnover and biomechanical competence

BV/TV (%) was significantly increased in 1-month old *Lgals3*$^{-/-}$ mice compared with WT littermates (Figure 1A-C). The increase in BV/TV (%) was due to an increase in Tb.N (Figure 1D), which was paralleled by reduced Tb.S (Figure 1E). Conversely, a reduction of BV/TV (%) and Tb.N , and an increase in Tb.S were observed in 3-month old *Lgals3*$^{-/-}$ compared with coeval WT mice (Figure 1C-E). These structural differences between the two genotypes were maintained at 6 months of age, although to a lesser extent.

Ct.Th (Figure 2A-C), TA, BA, TA/BA, and Ix (data not shown) were similar between the two genotypes at all ages evaluated. Nevertheless, biomechanical analysis revealed reduced femoral bending strength in *Lgals3*$^{-/-}$, as demonstrated by the reduced ultimate force values (N) for three-point bending tests of femora from 3 weeks old *Lgals3*$^{-/-}$ compared to WT mice (Figure 2D).

Number of osteoblasts per bone perimeter and MAR were lower in 3-month old *Lgals3*$^{-/-}$ vs coeval WT mice (Figure 3A-C). Conversely, osteoclast number was significantly increased at 1 month and showed a trend toward reduction at 3 and 6 months in *Lgals3*$^{-/-}$ mice (Figure 3D-E). Finally, IHC showed an increased number of F4/80 positive cells in bones from 3 months old *Lgals3*$^{-/-}$ compared with age-matched WT mice (Figure 3F-G).

The circulating levels of the bone remodeling markers TRAcP 5b, ucOCN and CTX were increased in 1-month old *Lgals3*$^{-/-}$ vs coeval WT mice (Figure 4A-C). Levels of ucOCN decreased with age in both genotypes, though the reduction was greater in *Lgals3*$^{-/-}$ mice; nevertheless, ucOC remained significantly higher in *Lgals3*$^{-/-}$ vs WT mice also at 3 months of age, as did CTX levels (Figure 4B-C). Conversely, OCN levels were significantly lower in *Lgals3*$^{-/-}$ vs WT at 3 and 6 months of age (Figure 4D).

3.2 *Lgals3*$^{-/-}$ mice show altered skeletal gene expression of osteogenic and inflammatory markers

Lgals3$^{-/-}$ mice showed altered expression levels of several osteogenic markers, particularly those of osteoblasts, such as *Alpl*, *Runx2*, *Ocn*, *Opg/Rankl* (Figure 5). Specifically, *Alpl* was reduced in *Lgals3*$^{-/-}$ vs WT mice at 1, 3, and 6 months of age, *Ocn* expression in *Lgals3*$^{-/-}$ mice was 1/3 of that of WT animals at 3 and 6 months of age, *Opg* was reduced at 1 and 3 months, whereas *Runx* and *Rankl* were significantly reduced only at 3 months and 1 month, respectively. The osteoclast marker *Trap* was also reduced in *Lgals3*$^{-/-}$ mice at 3 months of age. Conversely, *Sost* expression in bone was almost twice in 3-months old *Lgals3*$^{-/-}$ compared with WT mice. Moreover, the expression of the inflammatory markers *Il6* and *Il1β* was significantly higher in *Lgals3*$^{-/-}$ vs WT mice at all ages considered (Figure 5). The mRNA levels of the macrophage marker *Adgre1* (F4/80) were higher at 3 months, whereas those of *Tgf-β* and *Il10* were lower at 1 and 3 months in *Lgals3*$^{-/-}$ vs WT mice (Supplementary Figure 1A-C). The levels of all these targets were below the method detectable limit at 6 months of age.

3.3 Calvarial osteoblasts from *Lgals3*$^{-/-}$ mice show reduced differentiation capacity and impaired WNT/β-catenin signaling

Calvarial osteoblasts were collected from *Lgals3*$^{-/-}$ and WT mice to obtain primary osteoblast cultures. *Lgals3*$^{-/-}$ osteoblasts showed reduced basal (i.e., in standard, non-osteogenic medium) mRNA expression of *Alpl*, *Ocn* and *Opg*, and increased mRNA levels of *Runx2* and *Rankl*, whereas *Col1a1* gene expression was similar in *Lgals3*$^{-/-}$ and WT cells (Figure 6A). Osteoblasts grown in osteogenic medium for 4 weeks revealed the greatest differences between the two genotypes, with *Lgals3*$^{-/-}$ osteoblasts showing dramatically diminished expression of all the above mentioned genes compared with WT cells, except for *Rankl*, the levels of which were higher in *Lgals3*$^{-/-}$ osteoblasts (Figure 6B).

The altered gene expression in *Lgals3*$^{-/-}$ osteoblasts during osteogenic induction was associated with impaired WNT/β-catenin signaling, as revealed by the luciferase activity measured 48h post-transfection of the TCF/LEF luciferase reporter vector (Figure 6C), as well as with decreased osteoblast activity and function, as reveled by the reduced *in vitro* osteoblast ALPL activity (Figure 6D) and impaired mineralization (Figure 6D), respectively. Altered mineralization was confirmed by the reduced total calcified area and total calcium content, with more numerous nodules of smaller size in *Lgals3*$^{-/-}$ vs WT monolayers (Supplementary Figure 2A-D). Finally, time course analysis of galectin-3 expression in WT osteoblasts grown in osteogenic medium revealed an up-and-down trend between time 0 and week four (Supplementary Figure 2E).

3.4. Osteoclast precursors from *Lgals3*$^{-/-}$ mice show increased number, altered maturation and reduced resorption activity

Quantification of the number of osteoclasts revealed an increased number of total and medium osteoclasts (i.e., osteoclasts with 4-10 nuclei) and a reduced number of large osteoclasts (i.e., mature osteoclasts with more than 10 nuclei) in *Lgals3*$^{-/-}$ vs WT mice (Figure 7A-B). The number of small osteoclasts (no more than 3 nuclei) did not differ between the two genotypes.

Analysis of osteoclast function by bone resorption assay showed reduced RANKL-induced total resorbed area in *Lgals3*$^{-/-}$ compared with WT cells, thought the number of resorption pits was greater in *Lgals3*$^{-/-}$ vs WT cultures (Figure 7C-E).

4. Discussion

The bulk of research on disorders of bone remodeling is focused on the two arms of the process, i.e., bone resorption by osteoclasts and bone formation by osteoblasts [1]. However, bone metabolism is more complex than a two-step-process and there is still a lot to be learned

about cellular and molecular mechanisms involved in skeletal remodeling. Particularly, imbalance between bone resorption and bone formation leading to reduced bone mass might be the results of multifaceted events affecting simultaneously osteoblasts, osteoclasts and, possibly, other bone cell populations.

Here, we identify galectin-3 as an essential factor in the regulation of both osteoblast and osteoclast differentiation, maturation and function.

4.1 Galectin-3 is an essential factor in the regulation of bone remodeling and biomechanical competence

Using *Lgal-3*$^{-/-}$ mice, we showed that galectin-3 ablation leads to disrupted bone remodeling and accelerated age-dependent trabecular bone loss. We also demonstrated that galectin-3 ablation is associated with reduced bone strength in the absence of significant changes in Ix, Ct.Th, and other geometric features of cortical bone possibly affecting its bending properties, indicating that the decreased biomechanical competence was mainly due to reduced bone quality. This assumption is also supported by previous observations indicating that *Lgals3*$^{-/-}$ mice display irregular extracellular matrix structure consisting in loss and reduced length of collagen fibers [38]. In addition, we obtained *in vitro* data demonstrating disrupted terminal differentiation/maturation of osteoblasts and osteoclasts derived from *Lgal-3*$^{-/-}$ mice, which were associated with impaired mineralization capacity and resorption activity, respectively. Finally, we found that bone phenotypic, biomechanical and remodeling abnormalities of *Lgal-3*$^{-/-}$ mice were associated with increased bone expression of inflammatory cytokines and, only at 3 months, osteal tissue macrophage content. Conversely, the bone expression levels of cytokines and M2 macrophage markers [39] were reduced in *Lgal-3*$^{-/-}$ vs WT mice.

At 1 month of age, *Lgals3*$^{-/-}$ mice showed a bone phenotype characterized by a transient increase in trabecular and cortical bone indices. This finding is consisted with a previous report showing that galectin-3 deletion resulted in defective epiphyseal growth plate of developing

long bones, suggesting a role for this lectin in the process of endochondral ossification during embryogenesis as a regulator of chondrocyte activity and survival [38].

Conversely, at 3 and, to a lesser extent, 6 months of age, BV/TV (%) was reduced in *Lgals3*$^{-/-}$ mice vs WT mice, indicating an early, accelerated age-dependent reduction in bone mass which suggests a role for galectin-3 also in the regulation of bone cell differentiation and activity. Increased loss of bone mass in *Lgals3*$^{-/-}$ mice between 1 and 3 months was associated with higher circulating levels of biochemical markers of bone turnover, such as TRAcP 5b (only at 1 month) and particularly CTX and ucOC, the product of OCN decarboxylation at the site of resorption [35] (at both 1 and 3 months). The unchanged (1 month) and reduced (3 and 6 months) *Ocn* expression and OCN serum levels in *Lgals3*$^{-/-}$ mice support the assumption that the increased ucOC serum levels observed at 1 and 3 months in *Lgals3*$^{-/-}$ mice were mainly dependent on an increased bone resorption. Conversely, the expression of sclerostin (*Sost*), an inhibitor of osteoblast activity secreted by old osteocytes [40,41], peaked at 3 months, concurrently with reduced bone formation. Microscopically, static and dynamic parameters showed a reduced number and function (MAR) of osteoblasts at 3 months and a transient increase in the number of osteoclasts at 1 month of age.

Altogether, these data suggest that the accelerated age-dependent bone loss observed in *Lgals3*$^{-/-}$mice was due not only to reduced bone formation, but also to increased bone resorption. Bone inflammation, as attested by the increased expression of the inflammatory cytokines *Il6* and *Il1β* in *Lgals3*$^{-/-}$mice, might have also contributed to bone loss by perturbation of the signals that coordinate physiological coupling of osteoclast and osteoblast activities [26,42]. Yet, the *in vivo* and *in vitro* analysis suggested reduced maturation and activity of osteoclasts. Indeed, bone *Trap* expression was lower at 3 months, consistent with the observed trend of a reduction of osteoclast number in *Lgals3*$^{-/-}$ mice of this age. Moreover, *in vitro* data showed impaired maturation and function of osteoclast precursors isolated from *Lgals3*$^{-/-}$ mice. Therefore, it seems unlikely that the increase in bone resorption depended exclusively on

osteoclast activity and/or number and it is conceivable that the inflammatory milieu might have favored bone resorption also through other bone cell populations. Indeed, we found higher mRNA expression of the macrophage marker F4/80 (*Adgre1*) and an increased number of macrophages in bones of 3 months-old *Lgals3*$^{-/-}$ mice. Osteal macrophages were recently shown to play a role in bone metabolism, sustaining physiologic skeletal remodeling and the anabolic actions of parathyroid hormone [43]. However, it is well known that genetic, environmental or immune-related factors influence the nature and function of macrophages. Therefore, it cannot be ruled out the possibility that functional defects of cells of the monocyte/macrophage lineage might impair bone homeostasis [44]. For instance, the polarization of osteal macrophages might affect bone biology and metabolism in opposite ways, consistent with the role of macrophage subpopulations in the pathophysiology of various inflammatory diseases [12]. Consistently, macrophage heterogeneity was shown to modulate also vascular calcification by favoring either mineral deposition (M2 macrophages) or resorption (M1 macrophages) [45]. Noteworthy, as mentioned above, galectin-3 sustains alternative (M2) macrophage activation [17,18]; accordingly, the bone expression levels of the M2 macrophage marker *Tgfb* and the anti-inflammatory cytokine *Il10* were reduced in *Lgals3*$^{-/-}$ mice. Therefore, these *in vivo* data suggest new galectin-3 functions in bone cells, including osteal macrophages, which could expand our knowledge on the cellular and molecular mechanisms involved in bone remodeling [46].

4.2 Galectin-3 regulates both osteoblast and osteoclast differentiation, maturation and function

The *in vitro* experiments confirmed the central role of galectin-3 in osteoblast biology and function. Deletion of *Lgals3*$^{-/-}$ resulted in dysregulated osteoblast differentiation and activity, as indicated by the altered expression pattern of several osteogenic genes, which was associated with diminished mineralization capacity. Mechanistically, the impaired differentiation and

function of *Lgals3*$^{-/-}$ osteoblasts was associated with altered WNT/β-catenin signaling, which is consistent with the key role of galectin-3 as a regulator of the WNT/β-catenin signaling pathway by virtue of its ability to interact with and translocate β-catenin into the nucleus [47].

Our experiments also demonstrated a role for galectin-3 in osteoclast differentiation and maturation. In fact, we observed increased osteoclast differentiation, but defective *in vitro* maturation and activity of bone marrow progenitors derived from *Lgals3*$^{-/-}$ mice. However, the osteoclast abnormalities observed *in vivo* might also be secondary to osteoblast dysfunction, possibly via the perturbation of the RANKL/OPG system.

4.3. Translational potential

Overall, our study identify galactin-3 as an attractive potential therapeutic target in some bone pathologies, primarily age-dependent disorders of bone remodeling. This concept is supported by the finding that, in addition to participating in endochondral ossification [6], galectin-3 is essential for proper bone cell differentiation and activity, bone remodeling and biomechanical competence. Moreover, the observation that *Lgals3* ablation is associated with an increased expression of pro-inflammatory cytokines in bone should prompt further studies investigating the potential of this lectin to favor resolution of chronic inflammatory disorders of the bones and joints.

4.4 Strengths and Weaknesses

Strengths of this study include the analysis of the skeletal phenotype of *Lgals3*$^{-/-}$ mice of different ages, which allowed us to get information on the role of galectin-3 in both growth and age-dependent changes of the bony structure. Moreover, the analysis of primary bone cells enabled us to demonstrate that the ablation of this lectin directly affects osteoblast and osteoclast differentiation and function. A weakness of the study is that we used total body instead of bone-specific knockout mice. Because of this limitation, we could not rule out the possibility that the net effect of *Lgals3* ablation on bone phenotype and function may be

dependent not only on bone cell dysfunction but also on an alteration of systemic regulation of bone metabolism.

5. CONCLUSIONS

This study provides evidence for a contribution of galectin-3 to bone cell maturation and function, bone remodeling, and biomechanical competence. Consistently, ablation of *Lgals3*$^{-/-}$ resulted in altered bone phenotype, reduced bone strength, and accelerated age-related trabecular bone loss, due to both impaired bone formation and increased bone resorption. The reduced bone formation was due to impaired osteoblast differentiation and function mediated by defective WNT/β-catenin signaling. Conversely, the increased bone resorption could be partly independent on osteoclast activity and prompts further investigation on the role of macrophage heterogeneity in bone remodeling and accelerated loss of bone mass.

Acknowledgements

The Authors thank Cinzia Cataldo for technical assistance in histology processing.

Funding: This work was supported by a research grant of the Research Foundation of the Italian Diabetes Society (Diabete Ricerca 2013) and Sapienza University of Rome - Progetti di Ateneo 2013 to SM.

Disclosure statement: The Authors declare no conflicts of interest.

Author contributions: CI, GP and SM contributed to conception and design, acquisition of data, analysis and interpretation of data and drafting the article; CP, CBF and AB contributed to acquisition of histological, biochemical and molecular data and critical revision of the article for important intellectual content; BA contributed to the conduction of *in vivo* experiments and

data collection; RP and RB conducted micro-computed tomography analysis and biomechanical tests. All authors gave final approval of the version to be published.

References

1. Rachner TD, Khosla S, Hofbauer LC. Osteoporosis: now and the future. *Lancet.* 2011;**377**:1276-1287.
2. Ducy P, Amling M, Takeda S, et al. Leptin inhibits bone formation through a hypothalamic relay: a central control of bone mass. *Cell*. 2000;**100**:197-207.
3. Delaisse JM. The reversal phase of the bone-remodeling cycle: cellular prerequisites for coupling resorption and formation. *Bonekey Rep.* 2014;**3**:561.
4. Lewiecki EM, Binkley N. What we don't know about osteoporosis. *J Endocrinol Invest.* 2016;**39**:491-493.
5. Blume SW, Curtis JR. Medical costs of osteoporosis in the elderly Medicare population. *Osteoporos Int.* 2011;**22**:1835-1844.
6. Colnot C, Sidhu SS, Poirier F, et al. Cellular and subcellular distribution of galectin-3 in the epiphyseal cartilage and bone of fetal and neonatal mice. *Cell Mol Biol.* 1999;**45**:1191-1202.
7. Iacobini C, Amadio L, Oddi G, et al. Role of galectin-3 in diabetic nephropathy. *J Am Soc Nephrol.* 2003;**14**:S264–S270.
8. Pugliese G, Pricci F, Iacobini C, et al. Accelerated diabetic glomerulopathy in galectin-3/AGE-receptor-3 knockout mice. *FASEB J.* 2001;**15**:2471–2479.
9. Iacobini C, Menini S, Ricci C, et al. Accelerated lipid-induced atherogenesis in galectin-3-deficient mice: role of lipoxidation via receptor-mediated mechanisms. *Arterioscler Thromb Vasc Biol.* 2009;**29**:831-836.

10. Kadoglou NP, Sfyroeras GS, Spathis A, et al. Galectin-3, Carotid Plaque Vulnerability, and Potential Effects of Statin Therapy. *Eur J Vasc Endovasc Surg.* 2015;**49**:4-9.

11. Li YJ, Kukita A, Teramachi J, et al. A possible suppressive role of galectin -3 in upregulated osteoclastogenesis accompanying adjuvant-induced arthritis in rats. *Lab Invest.* 2009;**89**:26-37.

12. Pugliese G, Iacobini C, Pesce CM, et al. Galectin-3: an emerging all-out player in metabolic disorders and their complications. *Glycobiology.* 2015;**25**:136-150.

13. Norling LV, Perretti M, Cooper D. Endogenous galectins and the control of the host inflammatory response. *J Endocrinol.* 2009;**201**:169-184.

14. Fukumori T, Takenaka Y, Yoshii T, et al.. CD29 and CD7 mediate galectin-3-induced type II T-cell apoptosis. *Cancer Res.* 2003;**63**:8302-8311.

15. Morgan R, Gao G, Pawling J, et al. N-acetylglucosaminyltransferase V (Mgat5)-mediated N-glycosylation negatively regulates Th1 cytokine production by T cells. *J Immunol.* 2004;**173**:7200-7208.

16. M. Demetriou, M. Granovsky, S. Quaggin, et al. Negative regulation of T-cell activation and autoimmunity by Mgat5 N-glycosylation. *Nature.* 2001;**409**:733–739.

17. MacKinnon AC, Farnworth SL, Hodkinson PS, et al. Regulation of alternative macrophage activation by galectin-3. *J Immunol.* 2008;**180**:2650-2658.

18. Kianoush F, Nematollahi M, Waterfield JD, et al. Regulation of RAW264.7 Macrophage Polarization on Smooth and Rough Surface Topographies by Galectin-3. *J Biomed Mater Res. A.* 2017 May 12. [Epub ahead of print]

19. Liu FT, Patterson RJ, Wang JL. Intracellular functions of galectins. *BBA-General Subjects.* 2002;**1572**:263–273.

20. Menon RP and Hughes RC. Determinants in theN-terminal domains of galectin-3 for secretion by a novel pathway circumventing the endoplasmic reticulum-Golgi complex. *Eur J Biochem.* 1999;**264**:569–576.

21. Dennis JW, Nabi IR, Demetriou M. Metabolism, cell surface organization, and disease. *Cell.* 2009;**139**:1229–1241.

22. Partridge EA, Le Roy C, Di Guglielmo GM, et al. Regulation of cytokine receptors by golgi N-glycan processing and endocytosis. *Science*. 2004;**306**:120-124.

23. Lakshminarayan R, Wunder C, Becken U, et al. Galectin-3 drives glycosphingolipid-dependent biogenesis of clathrinin-dependent carriers. *Nat Cell Biol.* 2014;**16**:595–606.

24. Menini S, Iacobini C, Ricci C, et al. The galectin-3/RAGE dyad modulates vascular osteogenesis in atherosclerosis. *Cardiovasc Res.* 2013;**100**:472-480.

25. Stock M, Schäfer H, Stricker S, et al. Expression of galectin-3 in skeletal tissues is controlled by Runx2. *J Biol Chem.* 2003;**278**:17360-17367.

26. Simon D, Derer A, Andes FT, Lezuo P, Bozec A, Schett G, Herrmann M, Harre U. Galectin-3 as a novel regulator of osteoblast-osteoclast interaction and bone homeostasis. *Bone*. 2017;**105**:35-41.

27. Iacobini C, Blasetti Fantauzzi C, Pugliese G, Menini S. Role of galectin-3 in bone cell differentiation, bone pathophysiology and vascular osteogenesis. *Int J Mol Sci*. 2017;**18**. pii: E2481.

28. Weilner S, Keider V, Winter M, et al. Vesicular Galectin-3 levels decrease with donor age and contribute to the reduced osteo-inductive potential of human plasma derived extracellular vesicles. *Aging.* 2016;**8**:16-33.

29. Lattanzi W, Parrilla C, Fetoni A, et al. Ex vivo-transduced autologous skin fibroblasts expressing human Lim mineralization protein-3 efficiently form new bone in animal models. *Gene Ther.* 2008;**15**:1330-1343.

30. Bouxsein ML, Boyd SK, Christiansen BA, Guldberg RE, Jepsen KJ, Müller R. Guidelines for assessment of bone microstructure in rodents using micro-computed tomography. *J Bone Miner Res*. 2010;25:1468-86.

31. Ritchie RO, Koester KJ, Ionova S, et al. Measurement of the toughness of bone: a tutorial with special reference to small animal studies. *Bone*. 2008;**43**:798-812.

32. ASTM Standard D 790-10. Flexural Properties of Unreinforced and Reinforced Plastics and Electrical Insulating Materials. American Society for Testing and Materials: West Conshohocken, Pennsylvania, USA 2010.

33. Parfitt AM, Drezner MK, Glorieux FH, et al. Bone histomorphometry: standardization of nomenclature, symbols, and units: report of the ASBMR Histomorphometry Nomenclature Committee. *J Bone Miner Res.* 1987;**12**:595–610.

34. Menini S, Iacobini C, Ricci C, et al. Protection from diabetes-induced atherosclerosis and renal disease by D-carnosine-octylester: effects of early vs late inhibition of advanced glycation end-products in Apoe-null mice. *Diabetologia.* 2015;**58**:845-853.

35. Ferron M, Wei J, Yoshizawa T, et al. Insulin signaling in osteoblasts integrates bone remodeling and energy metabolism. *Cell.* 2010;**142**:296-308.

36. Linkhart TA, Linkhart SG, Kodama Y, et al. Osteoclast formation in bone marrow cultures from two inbred strains of mice with different bone densities. *J Bone Miner Res.* 1999;**14**:39-46.

37. Caselli G, Mantovanini M, Gandolfi CA, et al. Tartronates: a new generation of drugs affecting bone metabolism. *J Bone Miner Res.* 1997;**12**:972-981.

38. Colnot C, Sidhu SS, Balmain N, et al. Uncoupling of chondrocyte death and vascular invasion in mouse galectin 3 null mutant bones. *Dev Biol.* 2001;**229**:203-214.

39. Rőszer T. Understanding the mysterious M2 macrophage through activation markers and effector mechanisms. *Mediators Inflamm.* 2015;**2015**:816460.

40. van Bezooijen RL, Roelen BA, Visser A, et al. Sclerostin is an osteocyte-expressed negative regulator of bone formation, but not a classical BMP antagonist. *J Exp Med.* 2004;**199**:805-814.

41. Sebastian A, Loots GG. Genetics of Sost/SOST in sclerosteosis and van Buchem disease animal models. *Metabolism*. 2017 Oct 25. pii: S0026-0495(17)30279-2. [Epub ahead of print].

42. Kwan Tat S, Padrines M, Théoleyre S, et al. IL-6, RANKL, TNF-alpha/IL-1: interrelations in bone resorption pathophysiology. *Cytokine Growth Factor Rev.* 2004;**15**:49-60.

43. Cho SW, Soki FN, Koh AJ, et al. Osteal macrophages support physiologic skeletal remodeling and anabolic actions of parathyroid hormone in bone. *Proc Natl Acad Sci USA.* 2014;**111**:1545-1550.

44. Pettit AR, Chang MK, Hume DA, et al. Osteal macrophages: a new twist on coupling during bone dynamics. *Bone.* 2008;**43**:976-982.

45. Rogers MA, Aikawa M, Aikawa E. Macrophage heterogeneity complicates reversal of calcification in cardiovascular tissues. *Circ Res.* 2017;**121**:5-7.

46. Polyzos SA, Mantzoros CS. Outliers of bone metabolic diseases. *Metabolism*. 2017 Oct 4. pii: S0026-0495(17)30261-5. [Epub ahead of print].

47. Shimura T, Takenaka Y, Fukumori T, et al. Implication of galectin-3 in Wnt signaling. *Cancer Res.* 2005;**65**:3535-3537.

Figure legends

Figure 1. Trabecular bone structure analysis at the distal femoral metaphysis.

Representative 2D μCT images of distal femoral metaphysis (A) and hematoxylin-eosin stained sections (B) of proximal tibiae of WT and *Lgals3*$^{-/-}$ female mice aged 1, 3 and 6 months; and quantification of bone volume/total tissue volume (BV/TV, C), trabecular number (Tb.N, D), trabecular separation (Tb.Sp, E) and trabecular thickness (Tb.Th, F) in WT (open bars) and *Lgals3*$^{-/-}$ (closed bars) female mice aged 1, 3 and 6 months. Results are the mean±SD of 5 mice per group. Scale bar, 400 μm. *P<0.05, **P<0.01 or ***P<0.001 vs WT.

Figure 2. Cortical bone structure analysis and biomechanical testing of the femurs.

Representative longitudinal (A) and cross-sectional (B) μCT images corresponding to the indicated position (red line) of femurs of WT and *Lgals3*$^{-/-}$ female mice aged 1, 3 and 6 months; quantification of bone cortical thickness (Ct.Th, C) of the femoral midshaft of WT (open bars; n=5) and *Lgals3*$^{-/-}$ (closed bars; n=5) female mice aged 1, 3 and 6 months; and three-point bending analysis of the femurs of 3-month old female WT (n=5) and *Lgals3*$^{-/-}$ (n=6) mice (D). **P<0.01 vs WT.

Figure 3. Static and dynamic bone histomorphometry and immunohistochemistry.

Number of osteoblasts (A), calcein double labeling from representative 3-month-old animals (B), and quantification of the mineral apposition rate (MAR) by morphometric analysis of calcein-labeled sections (C) in femurs from WT (open bars) and *Lgals3*$^{-/-}$ (closed bars) female mice aged 1, 3 and 6 months (calcein incorporates in newly calcifying bone; the distance between the two labels divided by time represents the MAR); histoenzymatic (TRAcP) and immunohistochemical (F4/80) detection of osteoclasts (E) and macrophages (F) from representative 1 and 3-month-old WT and *Lgals3*$^{-/-}$ mice; and quantification of osteoclast (D) and F4/80 positive cell (G) number in tibial bones from WT (open bars) and *Lgals3*$^{-/-}$ (closed

bars) female mice aged 1, 3 and 6 months. Scale bars, 20 μm in B and 100 μm in E and F. Results are the mean±SD of seven (1- and 3-month old) and six (6-month old) mice per genotype. *P<0.05 or **P<0.01 versus age-matched WT.

Figure 4. Serum bone turnover markers. Plasma levels of the bone remodeling markers TRAcP (A), ucOCN (B) CTX (C) and OCN (D) in WT (open bars) and *Lgals3*$^{-/-}$ (closed bars) female mice aged 1, 3 and 6 months. Results are the mean±SD of seven (1- and 3-month old) and six (6-month old) mice per genotype. *P<0.05, **P<0.01 or ***P<0.001 versus age-matched WT.

Figure 5. mRNA levels of osteogenic and inflammatory marker in bone. Quantitative real time-PCR analysis of the gene expression of osteogenic and inflammation markers in bones from WT (open bars) and *Lgals3*$^{-/-}$ (closed bars) female mice aged 1, 3 and 6 months. Results are the mean±SD of seven (1- and 3-month old) and six (6-month old) mice per genotype. *P<0.05, ***P*<0.01 or ****P*<0.001 versus age-matched WT.

Figure 6. *In vitro* analysis of osteoblastogenesis. Quantitative real time-PCR analysis of osteogenic markers in osteoblasts isolated from calvaria of WT (open bars) and *Lgals3*$^{-/-}$ (closed bars) mice cultured in standard (A) and osteogenic medium (B); analysis of the activity of the WNT/β-catenin pathway in primary osteoblast monolayers from WT (open bars) and *Lgals3*$^{-/-}$ (closed bars) mice grown in standard and osteogenic medium (C, values represent the mean±SD of the relative light units [RLU] of the firefly and renilla luciferase luminescence ratio of six biological replicates [three independent experiments in duplicate]); and representative images of the *in vitro* mineralization capacity (Von Kossa and Alizarin red staining) and ALP activity (D) of calvarial osteoblast from WT and *Lgals3*$^{-/-}$ mice. Values represent the mean±SD of at least three independent experiments. *P<0.05, **P<0.01 or ***P<0.001 versus WT; †P<0.001 vs standard medium.

Figure 7. ***In vitro*** **analysis of osteoclastogenesis**. Representative images of TRAcP staining of primary monocyte/macrophage cells grown in osteoclastogenic medium containing M-CSF and RANKL (A) and quantification of the number (N) of small, medium, large and total osteoclasts from long bones of WT (open bars) and *Lgals3*$^{-/-}$(closed bars) 6-week old female mice (B); representative images of bone resorption capacity of osteoclasts cultured on bone slices (C) and quantification of percent resorbed area/well (D) and number of pits/cm^2 (E) in cells from WT (open bars) and *Lgals3*$^{-/-}$(closed bars) mice. Scale bars, 10 μm in A and 100 μm in C. Values represent the mean±SD of at least three independent experiments. *P<0.05, **P<0.01 or ***P<0.001 versus WT.

Highlights

- Galectin-3 null (*Lgals3*$^{-/-}$) mice show accelerated age-dependent trabecular bone loss
- Lower bone formation and higher bone resorption were both observed in *Lgals3*$^{-/-}$ mice
- *Lgals3*$^{-/-}$ femurs display reduced bone strength likely due to poor bone quality
- Structural and functional bone abnormalities coexist with a steady inflammatory state
- *In vitro* differentiation/activity of *Lgals3*$^{-/-}$ osteoclast and osteoblast was impaired

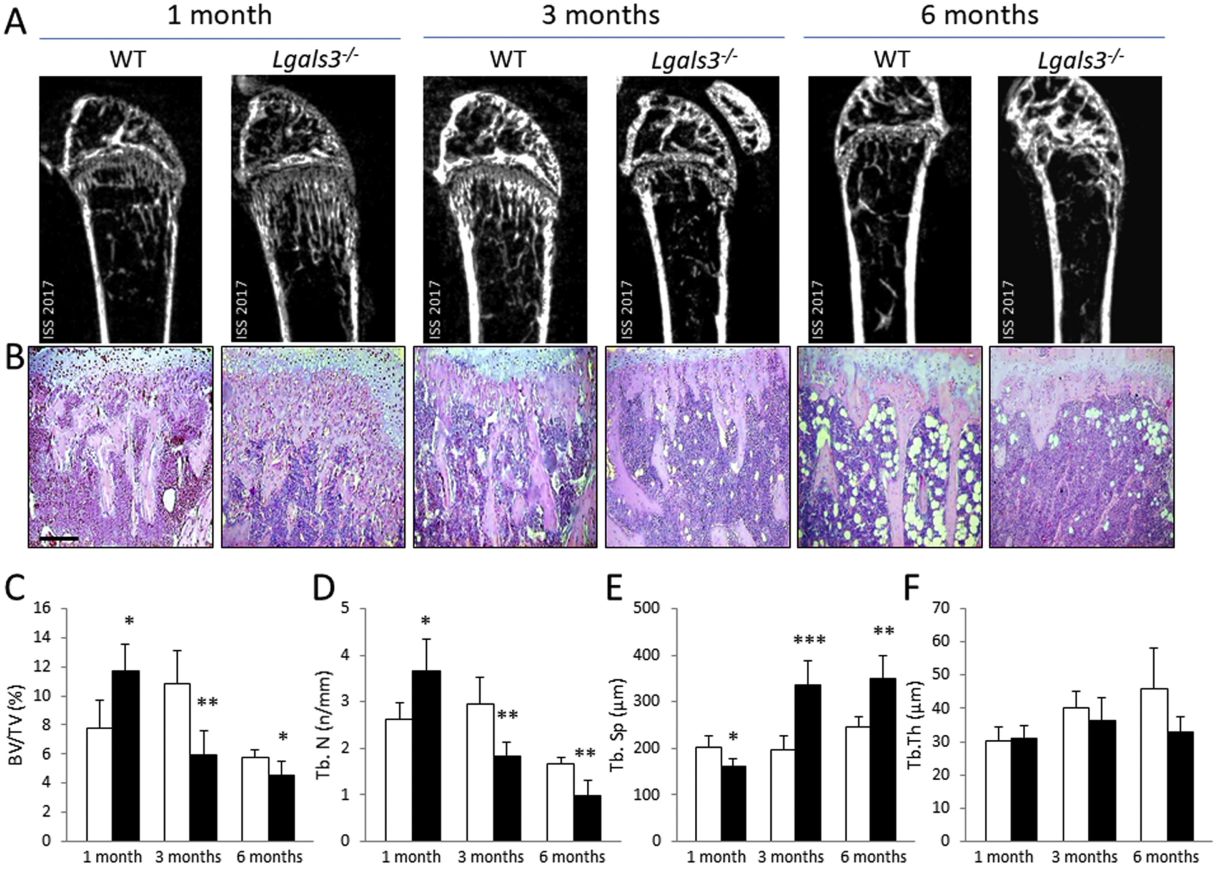
A
1 month
3 months
6 months
WT
Lgals3-/-
WT
Lgals3-/-
WT
Lgals3-/-
ISS 2017
B
C
BV/TV (%)
16
14
12
10
8
6
4
2
0
*
**
*
1 month
3 months
6 months
D
Tb. N (n/mm)
5
4
3
2
1
0
*
**
**
1 month
3 months
6 months
E
Tb. Sp (µm)
500
400
300
200
100
0
*
***
**
1 month
3 months
6 months
F
Tb.Th (µm)
70
60
50
40
30
20
10
0
1 month
3 months
6 months

Figure 1

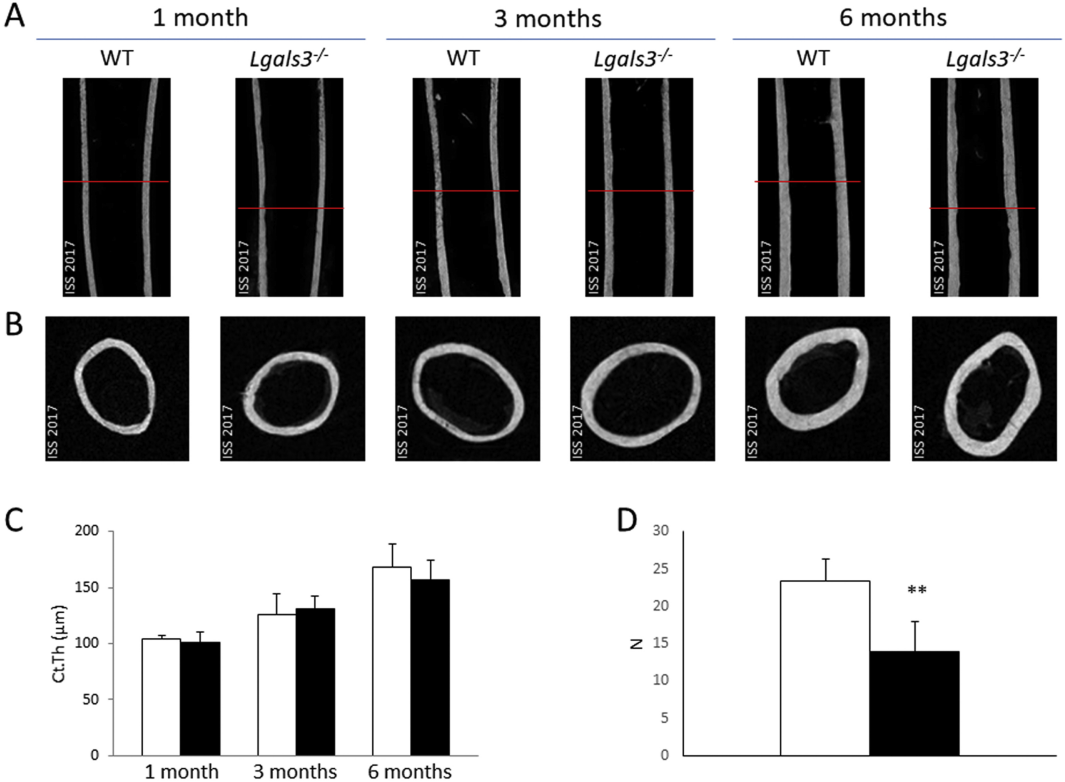
A
1 month
3 months
6 months
WT
Lgals3-/-
WT
Lgals3-/-
WT
Lgals3-/-
ISS 2017
B
C
Ct.Th (µm)
200
150
100
50
0
1 month
3 months
6 months
D
N
30
25
20
15
10
5
0
**

Figure 2

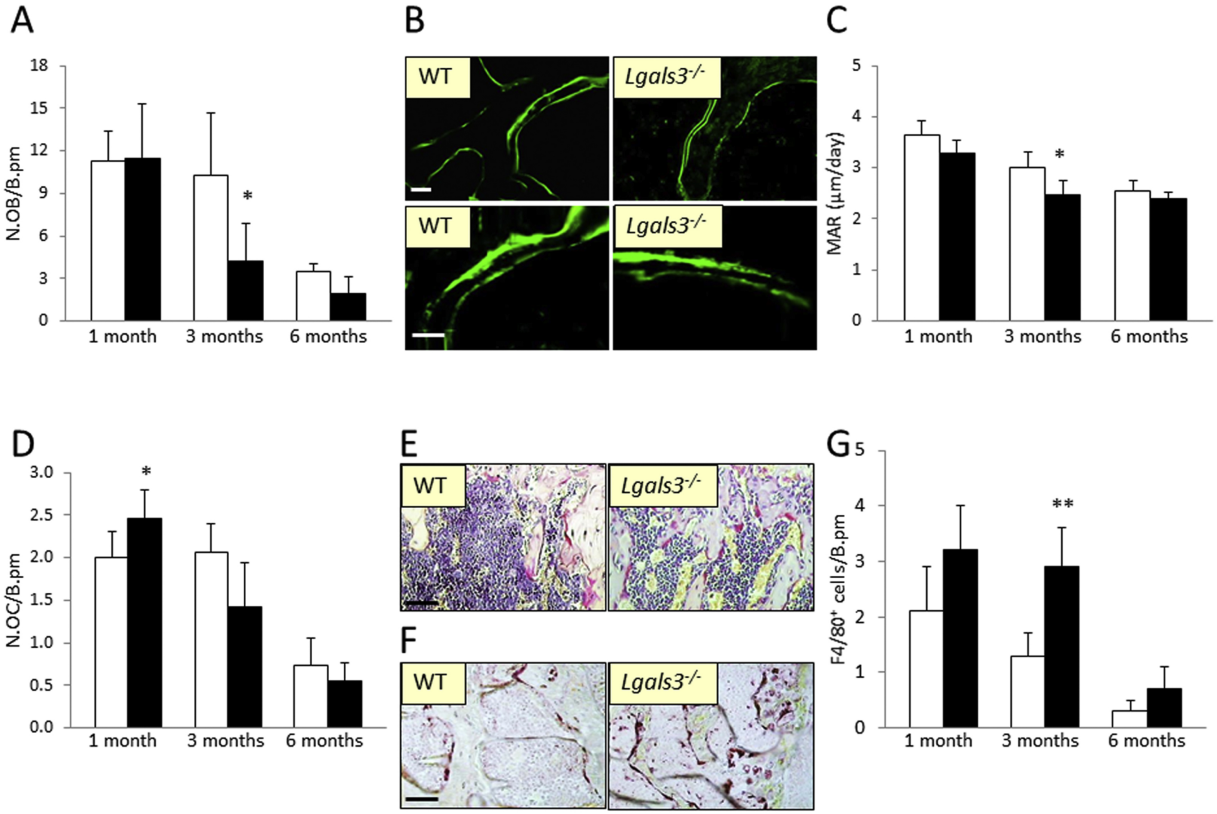
A
N.OB/B.pm
18
15
12
9
6
3
0
1 month
3 months
6 months
*
B
WT
Lgals3-/-
WT
Lgals3-/-
C
MAR (µm/day)
5
4
3
2
1
0
1 month
3 months
6 months
*
D
N.OC/B.pm
3.0
2.5
2.0
1.5
1.0
0.5
0.0
1 month
3 months
6 months
*
E
WT
Lgals3-/-
F
WT
Lgals3-/-
G
F4/80+ cells/B.pm
5
4
3
2
1
0
1 month
3 months
6 months
**

Figure 3

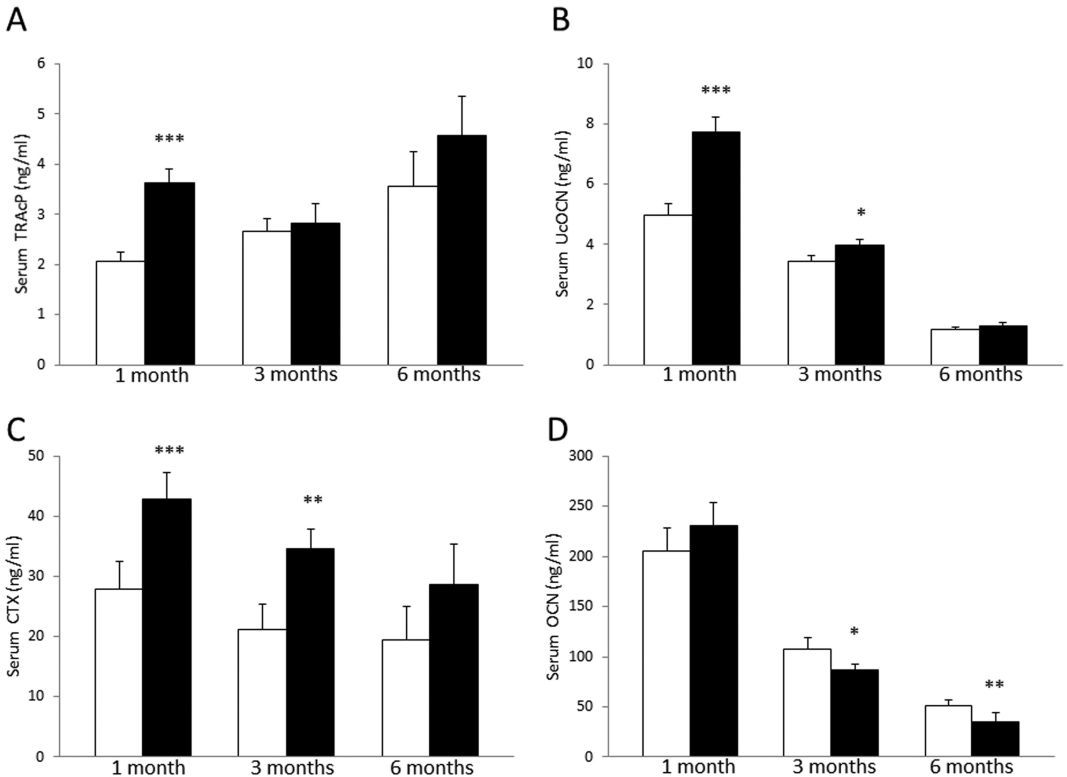
A
Serum TRAcP (ng/ml)
6
5
4
3
2
1
0
***
1 month
3 months
6 months
B
Serum UcOCN (ng/ml)
10
8
6
4
2
0
***
*
1 month
3 months
6 months
C
Serum CTX (ng/ml)
50
40
30
20
10
0
***
**
1 month
3 months
6 months
D
Serum OCN (ng/ml)
300
250
200
150
100
50
0
*
**
1 month
3 months
6 months

Figure 4

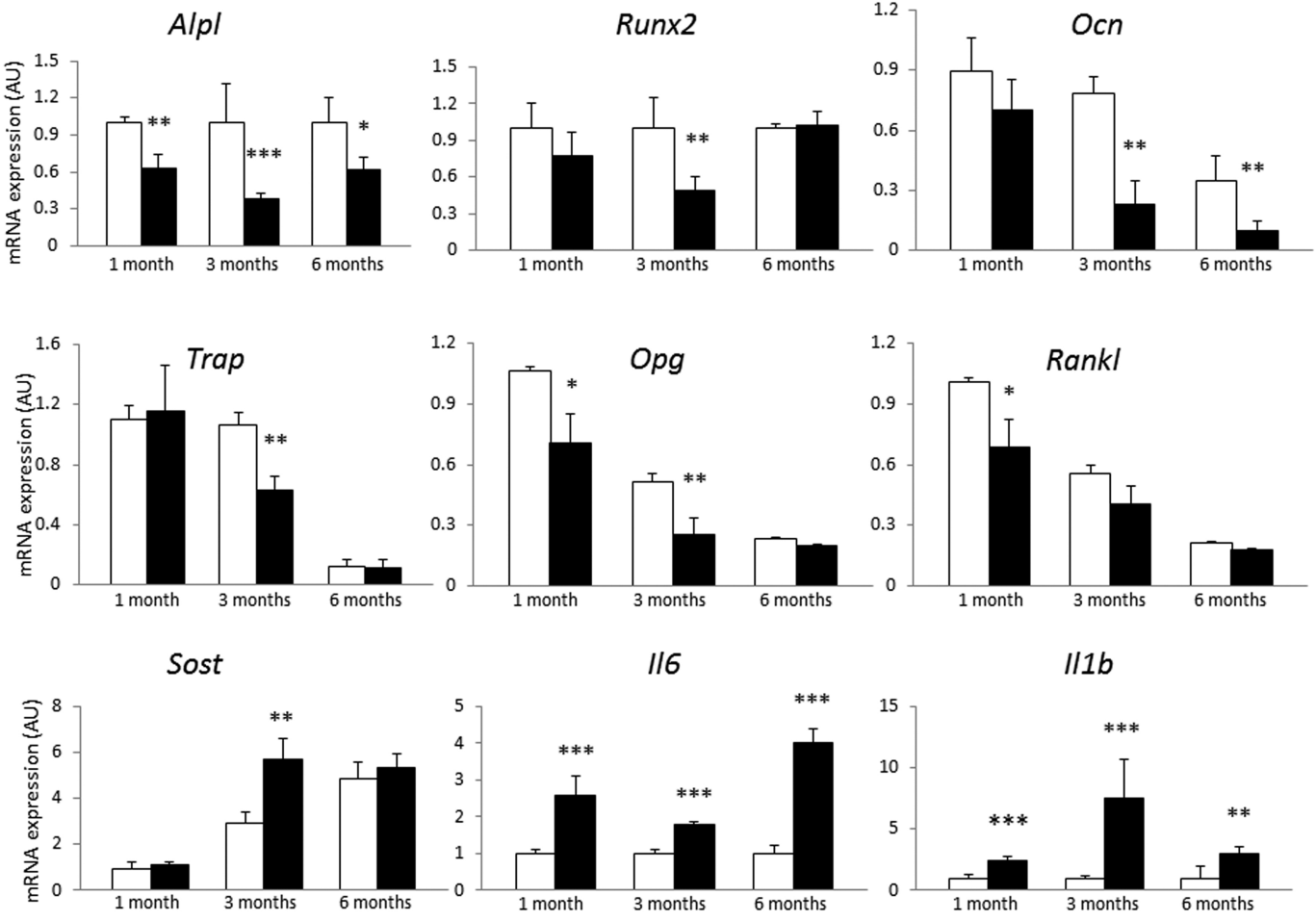
Alpl
Runx2
Ocn
Trap
Opg
Rankl
Sost
Il6
Il1b
mRNA expression (AU)
1 month
3 months
6 months

Figure 5

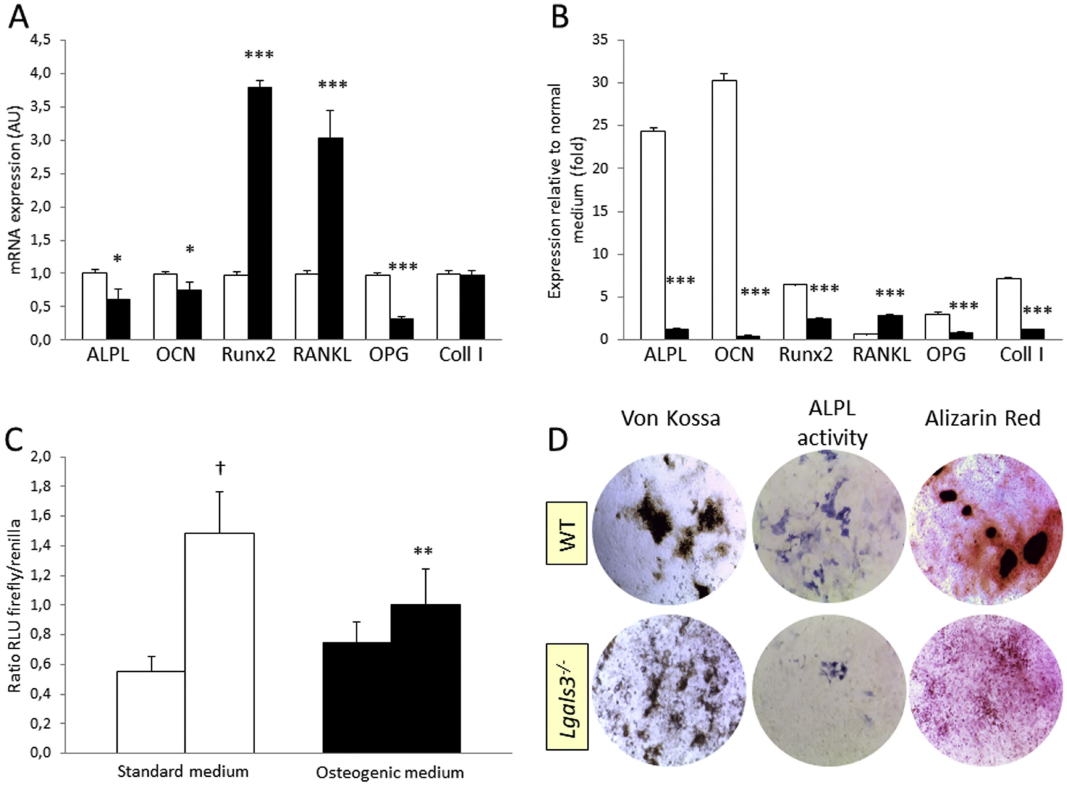
A
mRNA expression (AU)
4,5
4,0
3,5
3,0
2,5
2,0
1,5
1,0
0,5
0,0
*
*
***
***
***
ALPL
OCN
Runx2
RANKL
OPG
Coll I
B
Expression relative to normal medium (fold)
35
30
25
20
15
10
5
0
***
***
***
***
***
***
ALPL
OCN
Runx2
RANKL
OPG
Coll I
C
Ratio RLU firefly/renilla
2,0
1,8
1,6
1,4
1,2
1,0
0,8
0,6
0,4
0,2
0,0
†
**
Standard medium
Osteogenic medium
D
Von Kossa
ALPL activity
Alizarin Red
WT
Lgals3-/-

Figure 6

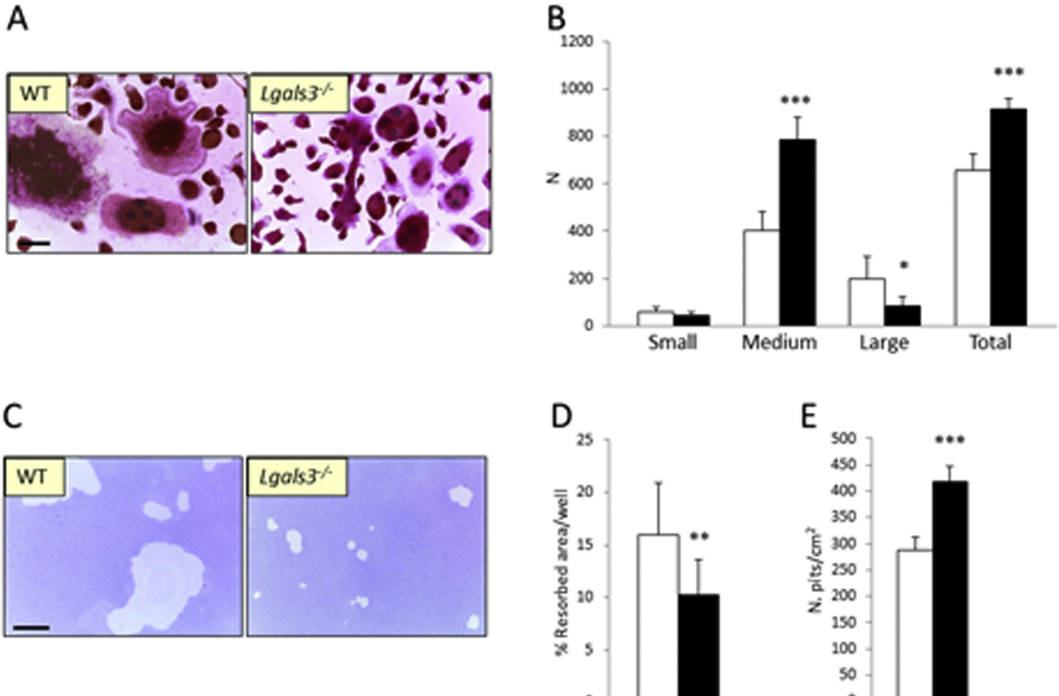
A
WT
Lgals3-/-
B
N
1200
1000
800
600
400
200
0
***
***
*
Small
Medium
Large
Total
C
WT
Lgals3-/-
D
% Resorbed area/well
25
20
15
10
5
0
**
E
N. pits/cm2
500
450
400
350
300
250
200
150
100
50
0
***

Figure 7